Lateral and Longitudinal Control of an Autonomous Unicycle*

Máté B. Vizi¹, Gábor Orosz², Dénes Takács³, and Gábor Stépán³

Abstract—Trajectory tracking with an autonomous unicycle is considered in three-dimensional space. It is shown that with the appropriate choice of pseudo-velocities the lateral and longitudinal dynamics and control can be decoupled at the linear level. Linear state feedback controllers are designed separately for lateral and longitudinal subsystems and these controllers are tested simultaneously for the nonlinear model via numerical simulations.

I. INTRODUCTION

Micro-mobility devices, such as electric unicycles and electric scooters, offer a convenient and efficient solution for short-distance commutes as an alternative to traditional forms of transportation. Consequently, these compact vehicles are quickly gaining popularity in urban environments and we can expect further increase in their presence.

The properties of these vehicles are also attractive for researchers in robotics where several autonomous unicycle designs have been developed in the last decades. Various approaches were taken to control the unicycles, for example using inverted pendulums [1], flywheels [2], [3], [4], gyroscopes [5] or combinations of those [6]. Even robotic arms were applied [7] and humanoid-type unicycles [8] were also developed. Nevertheless, the dynamical description of the nonholonomic mechanical systems, combined with motion planning and control design are still largely missing in the literature.

In this work, we extend our previous modeling efforts about the spatial dynamics of an autonomous unicycle [9], [10] to control not only the lateral but also the longitudinal dynamics while simultaneously balancing the payload, see Fig. 1. The lateral motion control is designed similarly to our previous work [9], [10], namely, the center of gravity is shifted sideways by moving a single point mass along the axle of the wheel. For the longitudinal motion control, the model is now extended by an (inverted) pendulum that is assumed to be a point mass at the end of a massless fork.

*The research reported in this paper was supported by the Hungarian National Science Foundation under Grant Nos. NKFI-K-132477 and NKFI-KKP-133846, and by the HUN-REN Hungarian Research Network. The research of DT was supported by a János Bolyai Research Scholarship of the Hungarian Academy of Sciences. GO acknowledges the support of the Hungarian Academy of Sciences within the Distinguished Guest Fellowship Programme and the support of the Fulbright Foundation.

¹M. B. Vizi is with the Department of Mechanical Engineering, University of Michigan, Ann Arbor, MI 48109, USA (e-mail: vizi@mm.bme.hu)

²G. Orosz is with the Department of Mechanical Engineering and with the Department of Civil and Environmental Engineering, University of Michigan, Ann Arbor, MI 48109, USA (e-mail: orosz@umich.edu).

³D. Takács, and G. Stépán are with the Department of Applied Mechanics, Budapest University of Technology and Economics, Budapest, Hungary and HUN-REN-BME Dynamics of Machines Research Group, Budapest, Hungary (e-mails: takacs@mm.bme.hu, stepan@mm.bme.hu)

The equations of motion are derived using the Appellian approach [11], which incorporates the kinematic (nonholonomic) constraints of rolling and yields a system of first-order ordinary differential equations for the configuration coordinates and pseudo-velocities. This provides the most compact representation of our nonholonomic mechanical system. For further details on the Appellian methodology, an interested reader may refer to [12], [13].

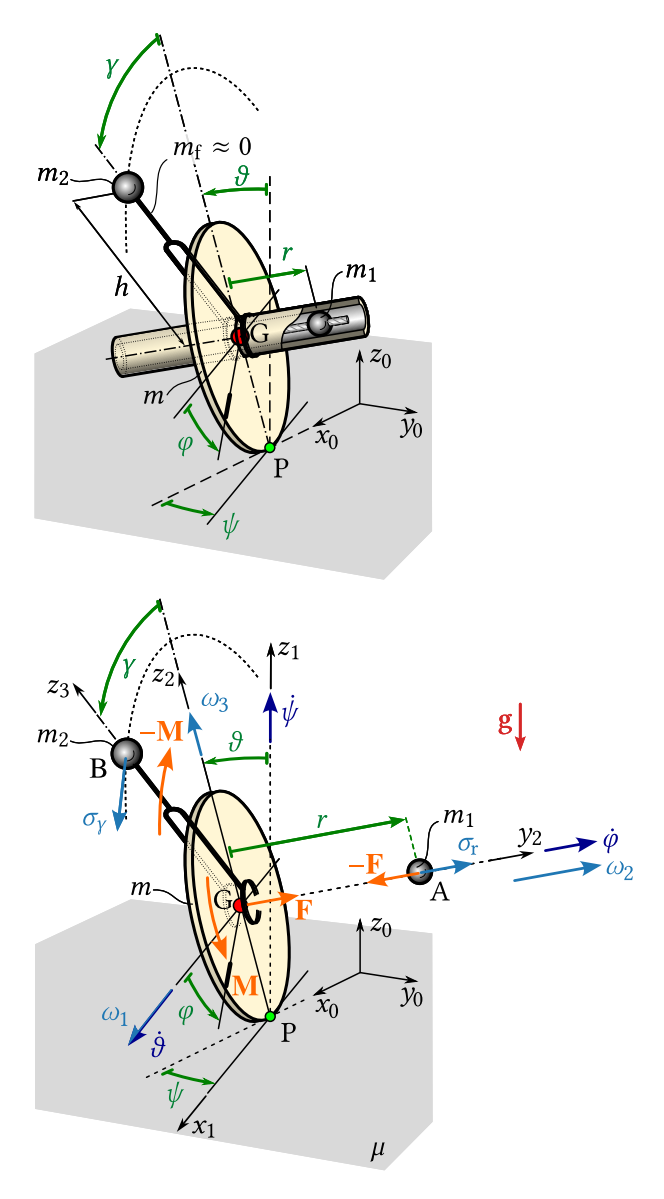


Fig. 1. Mechanical model and physical quantities

Our goal is to track a predefined path with the autonomous unicycle, so the model is transformed into a reference frame, which is moving along the path. Thus, the longitudinal, lateral, and alignment errors become system states; these are used in the control algorithm. It is shown that, with the appropriate choice of pseudo-velocities, the lateral and longitudinal dynamics can be decoupled when the system is linearized around the straight rolling steady state. Consequently, lateral and longitudinal feedback controllers can be developed independently. However, the lateral controller takes into account the velocity of the unicycle, which is a key factor due to its self-stabilizing effect [9]. Numerical simulations of the nonlinear system show that the designed controllers have good path-tracking performance and are able to balance the payload with small errors too.

II. GOVERNING EQUATIONS

The unicycle is modeled as a wheel (disc) with mass m and radius R, and two additional mass actuators. The point mass with mass m_1 can be moved perpendicularly to the wheel by the internal force

$$\mathbf{F} = \begin{bmatrix} 0 & F & 0 \end{bmatrix}_{\mathcal{F}_2}^{\mathsf{T}},\tag{1}$$

acting at the wheel center G, while the counter force $-\mathbf{F}$ acts at the point mass actuator.

Here the subscript \mathcal{F}_i means that a vector is resolved in the coordinate frame \mathcal{F}_i of coordinate axes (x_i, y_i, z_i) , see Fig. 1. Briefly, frame \mathcal{F}_0 is fixed to the ground; frame \mathcal{F}_1 travels and yaws with the wheel; \mathcal{F}_2 is attached to the axle and yaws and tilts with the wheel; while \mathcal{F}_3 is attached to the pendulum and it yaws, tilts and pitches with the fork.

The payload is modeled as an inverted pendulum comprised of a massless fork $(m_f \approx 0)$ and a point mass of m_2 . The pendulum can be rotated around the y_2 axis. The internal torque

$$\mathbf{M} = \begin{bmatrix} 0 & M & 0 \end{bmatrix}_{\mathcal{T}_2}^{\mathsf{T}},\tag{2}$$

acts at the wheel, while $-\mathbf{M}$ acts at the fork. The internal force F and torque M are considered to be control inputs for the lateral and longitudinal control objectives, respectively. The unicycle system consisting of the wheel and two actuators would have N = 6 + 3 + 3 = 12 degrees of freedom if we do not take into account the constraints.

The position of the wheel is given by its center point G:

$$\mathbf{r}_{G} = \begin{bmatrix} x_{G} & y_{G} & z_{G} \end{bmatrix}_{\mathcal{F}_{0}}^{\mathsf{T}}, \tag{3}$$

while its orientation is characterized by the yaw ψ , tilt ϑ and pitch φ angles, see Fig. 1. When the wheel rolls on the horizontal ground, the velocity of the contact point P is zero, that is,

$$\mathbf{v}_{\mathbf{P}} = \mathbf{0}.\tag{4}$$

This velocity can also be expressed by the transport formula $\mathbf{v}_P = \mathbf{v}_G + \boldsymbol{\omega} \times \mathbf{r}_{GP}$, where the velocity \mathbf{v}_G of the center point G, the angular velocity $\boldsymbol{\omega}$ of the wheel, and the relative

position \mathbf{r}_{GP} of the contact point P with respect to G are given by

$$\mathbf{v}_{G} = \dot{\mathbf{r}}_{G} = \begin{bmatrix} \dot{x}_{G} & \dot{y}_{G} & \dot{z}_{G} \end{bmatrix}_{\mathcal{F}_{0}}^{\mathsf{T}}, \quad \mathbf{r}_{GP} = \begin{bmatrix} 0 & 0 & -R \end{bmatrix}_{\mathcal{F}_{2}}^{\mathsf{T}} \\ \boldsymbol{\omega} = \begin{bmatrix} \dot{\vartheta} & \dot{\varphi} + \dot{\psi} \sin \vartheta & \dot{\psi} \cos \vartheta \end{bmatrix}_{\mathcal{F}_{2}}^{\mathsf{T}}.$$
 (5)

Equations (4)–(5) lead to two kinematic (nonholonomic) constraints

$$\dot{x}_{G} = \dot{\psi}R\cos\psi\sin\vartheta + \dot{\vartheta}R\sin\psi\cos\vartheta + \dot{\varphi}R\cos\psi,
\dot{y}_{G} = \dot{\psi}R\sin\psi\sin\vartheta - \dot{\vartheta}R\cos\psi\cos\vartheta + \dot{\varphi}R\sin\psi,$$
(6)

and one geometric (holonomic) constraint

$$\dot{z}_{\rm G} = -\dot{\vartheta}R\sin\vartheta \quad \Rightarrow \quad z_{\rm G} = R\cos\vartheta.$$
 (7)

The positions of the point masses m_1 and m_2 can be calculated by means of $\mathbf{r}_A = \mathbf{r}_G + \mathbf{r}_{GA}$ and $\mathbf{r}_B = \mathbf{r}_G + \mathbf{r}_{GB}$, respectively. The relative positions are

$$\mathbf{r}_{\mathrm{GA}} = \begin{bmatrix} 0 & r & 0 \end{bmatrix}_{\mathcal{T}_{2}}^{\mathsf{T}}, \qquad \mathbf{r}_{\mathrm{GB}} = \begin{bmatrix} 0 & 0 & h \end{bmatrix}_{\mathcal{T}_{3}}^{\mathsf{T}}, \qquad (8)$$

where r(t) is the (time dependent) position of the point mass m_1 along the wheel axle, while h is the (constant) length of the pendulum. These yield 2 + 2 = 4 additional geometric constraints.

Overall, we have $n_g = 5$ geometric and $n_k = 2$ kinematic constraints, so the unicycle forms a nonholonomic mechanical system. The Appellian approach is chosen for deriving the equations of motion due to its benefits shown in our previous works [9], [10].

First, $n_q = N - n_g = 7$ generalized coordinates q_k , with $k = 1, ..., n_q$ are selected, which can be used to unambiguously characterize the spatial configuration of the mechanical system; let these be:

$$x_{\rm G}, y_{\rm G}, \psi, \vartheta, \varphi, \gamma, r.$$
 (9)

The next step is to define $n_{\sigma} = N - n_{\rm g} - b_{\rm k} = 5$ pseudo-velocities σ_j , $j = 1, \ldots, n_{\sigma}$, which can be used to unambiguously express the derivatives of the generalized coordinates. These pseudo-velocities are denoted by

$$\omega_1, \ \omega_2, \ \omega_3, \ \sigma_r, \ \sigma_{\gamma}.$$
 (10)

The nontrivial pseudo-velocity definitions

$$\omega_{1} := \dot{\vartheta}, \qquad \omega_{2} := \dot{\varphi} + \dot{\psi} \sin \vartheta,
\omega_{3} := \dot{\psi} \cos \vartheta, \qquad \sigma_{r} := \dot{r} - \dot{\vartheta}R,
\sigma_{\gamma} := \dot{\gamma}h + \dot{\varphi}R \cos \gamma + \dot{\psi} (R \cos \gamma + h) \sin \vartheta$$
(11)

are used as these significantly reduce the algebraic complexity of the resulting equations of motion. The pseudo-velocities ω_1 , ω_2 , and ω_3 are the angular velocity components of the wheel resolved in frame \mathcal{F}_2 . The pseudo-velocity σ_r is the velocity component of the point mass m_1 along the axle (i.e., in the y_2 direction). Similarly, σ_γ is the velocity component of the point mass m_2 in the x_3 direction. Note that, the pseudo-velocities are the linear combinations of the generalized velocities.

From (6) and (11) the derivatives of the generalized coordinates (9) can be expressed as the linear combinations of the pseudo-velocities (10), these became

$$\dot{x}_{G} = \omega_{1}R\sin\psi\cos\vartheta + \omega_{2}R\cos\psi,$$

$$\dot{y}_{G} = -\omega_{1}R\cos\psi\cos\vartheta + \omega_{2}R\sin\psi,$$

$$\dot{\psi} = \omega_{3}/\cos\vartheta,$$

$$\dot{\vartheta} = \omega_{1},$$

$$\dot{\varphi} = \omega_{2} - \omega_{3}\tan\vartheta,$$

$$\dot{r} = \omega_{1}R + \sigma_{r},$$

$$\dot{\gamma} = -\omega_{2}(R/h)\cos\gamma - \omega_{3}\tan\vartheta + \sigma_{\gamma}/h.$$
(12)

The horizontal rest position $\vartheta = \pm \pi/2$ of the wheel leads to singularity, but this state is excluded from the analysis.

The next step is to calculate the acceleration energy of the unicycle:

$$S = S_{W} + S_{m_1} + S_{m_2}, \tag{13}$$

where the acceleration energies of the wheel, of the point mass m_1 at point A, and of the point mass m_2 at point B are calculated as

$$S_{w} = \frac{1}{2}m\mathbf{a}_{G}^{2} + \frac{1}{2}\boldsymbol{\alpha} \cdot \mathbf{J}_{G}\boldsymbol{\alpha} + \boldsymbol{\alpha} \cdot (\boldsymbol{\omega} \times \mathbf{J}_{G}\boldsymbol{\omega}),$$

$$S_{m_{1}} = \frac{1}{2}m_{1}\mathbf{a}_{A}^{2}, \qquad S_{m_{2}} = \frac{1}{2}m_{2}\mathbf{a}_{B}^{2}.$$
(14)

The acceleration of the wheel center G is

$$\mathbf{a}_{G} = \begin{bmatrix} R(\dot{\omega}_{2} + \omega_{1}\omega_{3}) \\ -R(\dot{\omega}_{1} - \omega_{2}\omega_{3}) \\ -R(\omega_{1}^{2} + \omega_{2}\omega_{3}\tan\vartheta) \end{bmatrix}_{\mathcal{T}_{2}},$$
(15)

the angular acceleration of the wheel is

$$\alpha = \begin{bmatrix} \dot{\omega}_1 - \omega_2 \omega_3 + \omega_3^2 \tan \vartheta \\ \dot{\omega}_2 \\ \dot{\omega}_3 + \omega_1 \omega_2 - \omega_1 \omega_3 \tan \vartheta \end{bmatrix}_{\mathcal{T}_2}, \tag{16}$$

and the mass moment matrix of inertia of the wheel about the center of gravity is

$$\mathbf{J}_{G} = \frac{mR^{2}}{4} \begin{bmatrix} 1 & 0 & 0 \\ 0 & 2 & 0 \\ 0 & 0 & 1 \end{bmatrix}_{\mathcal{F}_{2}}.$$
 (17)

The velocity and acceleration of point A are

$$\mathbf{v}_{A} = \begin{bmatrix} \omega_{2}R - \omega_{3}r & \sigma_{r} & \omega_{1}r \end{bmatrix}_{\mathcal{F}_{2}}^{\mathsf{T}},$$

$$\mathbf{a}_{A} = \begin{bmatrix} \dot{\omega}_{2}R - \dot{\omega}_{3}r + \omega_{1}\omega_{3}\left(r\tan\vartheta - R\right) - 2\omega_{3}\sigma_{r} \\ \dot{\sigma}_{r} - \omega_{1}^{2}r - \omega_{3}^{2}r + \omega_{2}\omega_{3}R \\ \dot{\omega}_{1}r + \omega_{1}^{2}R + 2\omega_{1}\sigma_{r} + (\omega_{3}^{2}r - \omega_{2}\omega_{3}R)\tan\vartheta \end{bmatrix}_{\mathcal{F}_{2}}^{\mathsf{T}},$$
(18)

while the velocity and acceleration of point B are expressed as

$$\mathbf{v}_{\mathrm{B}} = \begin{bmatrix} \sigma_{\gamma} \\ -\omega_{1}(R - h\cos\gamma) + \omega_{3}h\sin\gamma \\ \omega_{2}R\sin\gamma \end{bmatrix}_{\mathcal{F}_{3}}^{T},$$

$$\mathbf{a}_{\mathrm{B}} = \begin{bmatrix} a_{\mathrm{B}x} & a_{\mathrm{B}y} & a_{\mathrm{B}z} \end{bmatrix}_{\mathcal{F}_{3}}^{T},$$
(19)

where the vector components are

$$a_{\rm Bx} = \frac{1}{h} (\dot{\sigma}_{\gamma} h + \omega_1^2 (R + h \cos \gamma) h \sin \gamma - \omega_2^2 R^2 \sin \gamma \cos \gamma - \omega_3^2 h^2 \sin \gamma \cos \gamma + \omega_2 \sigma_{\gamma} R \sin \gamma + \omega_1 \omega_3 (R \cos \gamma + 2h \cos^2 \gamma - h) h),$$

$$a_{\rm By} = -\dot{\omega}_1 (R + h \cos \gamma) + \dot{\omega}_3 h \sin \gamma - \omega_3^2 h \cos \gamma \tan \vartheta - 2\omega_1 \omega_2 R \sin \gamma \cos \gamma - \omega_1 \omega_3 h \sin \gamma \tan \vartheta + \omega_2 \omega_3 (1 - 2\cos^2 \gamma) R + 2\omega_1 \sigma_{\gamma} \sin \gamma + 2\omega_3 \sigma_{\gamma} \cos \gamma,$$

$$a_{\rm Bz} = \frac{1}{h} (\dot{\omega}_2 R h \sin \gamma - \omega_1^2 (R + h \cos \gamma) h \cos \gamma - \sigma_{\gamma}^2 - \omega_2^2 R^2 \cos^2 \gamma - \omega_3^2 \sin^2 \gamma h^2 - \omega_2 \omega_3 R h \cos \gamma \tan \vartheta + 2R\sigma_{\gamma} \omega_2 \cos \gamma + \omega_1 \omega_3 (R \sin \gamma + 2 \sin \gamma \cos \gamma) h).$$

$$(20)$$

The last remaining step is to calculate the pseudo-forces Π_j , $j = 1, ..., n_{\sigma}$. These can be obtained from the virtual power of the active forces:

$$\delta P = \mathbf{G} \cdot \delta \mathbf{v}_{G} + \mathbf{G}_{A} \cdot \delta \mathbf{v}_{A} + \mathbf{G}_{B} \cdot \delta \mathbf{v}_{B} + \mathbf{F} \cdot \delta \mathbf{v}_{G}$$
$$-\mathbf{F} \cdot \delta \mathbf{v}_{A} + \mathbf{M} \cdot \delta \boldsymbol{\omega} - \mathbf{M} \cdot \delta \boldsymbol{\Omega} = \sum_{j=1}^{n_{\sigma}} \Pi_{j} \, \delta \sigma_{j} \,, \tag{21}$$

where G, G_A , G_B are the gravitational forces, δv_G , δv_A , δv_B are the virtual velocities of the respective points, $\delta \omega$ is the virtual angular velocity of the wheel, and

$$\delta \mathbf{\Omega} = \begin{bmatrix} \delta \omega_1 & \frac{1}{h} (\delta \sigma_{\gamma} - \delta \omega_2 R \cos \gamma) & \delta \omega_3 \end{bmatrix}_{\mathcal{T}_2}^{\mathsf{T}}, \qquad (22)$$

is the virtual angular velocity of the pendulum. The resulting pseudo-forces are expressed as

$$\Pi_{1} = -FR + mgR \sin \vartheta - m_{1}gr \cos \vartheta
+ m_{2}g (R + h \cos \gamma) \sin \vartheta ,$$

$$\Pi_{2} = M (R \cos \gamma + h) / h - m_{2}gR \sin \gamma \cos \gamma \cos \vartheta ,$$

$$\Pi_{3} = -m_{2}gh \sin \gamma \sin \vartheta ,$$

$$\Pi_{4} = -F - m_{1}g \sin \vartheta ,$$

$$\Pi_{5} = -M/h + m_{2}g \sin \gamma \cos \vartheta .$$
(23)

Finally, the equations of motion are formulated as

$$\frac{\partial S}{\partial \dot{\sigma}_{j}} = \Pi_{j}, \qquad j = 1, \dots, n_{\sigma},
\dot{q}_{k} = \sum_{i=1}^{n_{\sigma}} f_{kj} \dot{\sigma}_{j}, \qquad k = 1, \dots, n_{q},$$
(24)

where the coefficients f_{kj} are identified from (12). The equations of motion consist of $n_{\sigma} + n_{q} = 12$ first-order ordinary differential equations, which contains $n_{\sigma} = 5$ dynamical and $n_{q} = 7$ kinematic equations (12).

III. TRAJECTORY TRACKING FORMULATION

Our goal is to follow a trajectory on the ground with the wheel-ground contact point P'. The position of the wheel-ground contact point is described as

$$\mathbf{r}_{\mathbf{P}'} = \mathbf{r}_{\mathbf{G}} + \mathbf{r}_{\mathbf{G}\mathbf{P}'} = \begin{bmatrix} x_{\mathbf{P}'} & y_{\mathbf{P}'} & 0 \end{bmatrix}_{\mathcal{F}_0}^{\mathsf{T}}, \tag{25}$$

where $\mathbf{r}_{GP'} = \begin{bmatrix} 0 & 0 & -R \end{bmatrix}_{\mathcal{F}_2}^T$.

Note that the wheel-ground contact point P' is a geometric point that is located at the same position as the velocity pole (also called instantaneous center of velocities) P for a single time instance, that is $\mathbf{r}_{P'} = \mathbf{r}_P$. The velocity pole P is the material point of the wheel for which the kinematic constraint of rolling $\mathbf{v}_P = \mathbf{0}$ holds; see (4). However, using (3), (6), (12) and (25) the velocity of the wheel-ground contact point can be calculated as $\mathbf{v}_{P'} = \dot{\mathbf{r}}_{P'} = \begin{bmatrix} \dot{x}_{P'} & \dot{y}_{P'} & 0 \end{bmatrix}_{\mathcal{F}_0}^T$, where

$$\dot{x}_{P'} = \omega_2 R \cos \psi - \omega_3 R \tan \vartheta \cos \psi,
\dot{y}_{P'} = \omega_2 R \sin \psi - \omega_3 R \tan \vartheta \sin \psi,$$
(26)

which are generally non-zeros. More details about this pole changing velocity can be found in [14].

In order to properly formulate the path tracking control tasks, we follow the approach in [13], so the unicycle system is transformed into the reference frame (s, ε, θ) attached to the path, where s is the arc length along the trajectory, ε is the lateral error, and θ is the angular error shown in Fig. 2.

As explained in [10], the evolution of the variables s, ε , and θ can be given as

$$\dot{s} = \frac{1}{1 - \kappa \varepsilon} (\omega_2 R \cos \theta - \omega_3 R \cos \theta \tan \vartheta),
\dot{\varepsilon} = \omega_2 R \sin \theta - \omega_3 R \sin \theta \tan \vartheta,
\dot{\theta} = \frac{-1}{(1 - \kappa \varepsilon) \cos \vartheta} (\omega_2 R \kappa \cos \theta \cos \vartheta - \omega_3 (1 - \kappa \varepsilon + R \kappa \sin \vartheta \cos \theta)),$$
(27)

where $\kappa(s)$ is the signed curvature of the path. Zero curvature corresponds to a straight trajectory, while positive or negative values mean left or right turns, respectively.

The unicycle system can be transformed to the trajectory reference frame (s, ε, θ) by replacing the equations corresponding to \dot{x}_G , \dot{y}_G , and $\dot{\psi}$ in (12) with (27).

IV. CONTROL DESIGN

We suppose that we can control the unicycle and track various paths by the slight perturbation of the straight rolling steady state, so we linearize the equation of motion about this state while considering a steady state pitch rate $\dot{\varphi}_* = \omega_2$.

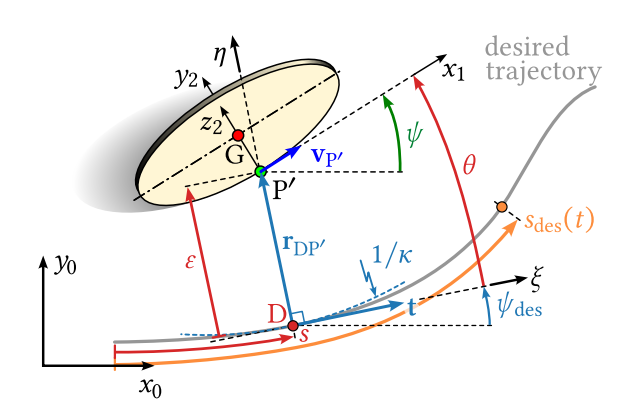


Fig. 2. Coordinate transformation to path coordinates

The linearized equation of motion has the form

$$\begin{bmatrix} \dot{\mathbf{x}}_{\text{lat}} \\ \dot{\mathbf{x}}_{\text{lon}} \end{bmatrix} = \begin{bmatrix} \mathbf{A}_{\text{lat}} & \mathbf{0} \\ \mathbf{0} & \mathbf{A}_{\text{lon}} \end{bmatrix} \begin{bmatrix} \mathbf{x}_{\text{lat}} \\ \mathbf{x}_{\text{lon}} \end{bmatrix} + \begin{bmatrix} \mathbf{B}_{\text{lat}} & \mathbf{0} \\ \mathbf{0} & \mathbf{B}_{\text{lon}} \end{bmatrix} \begin{bmatrix} u_{\text{lat}} \\ u_{\text{lon}} \end{bmatrix}, \quad (28)$$

that is, the lateral and longitudinal dynamics are decoupled. The corresponding state variables and the control inputs are

$$\mathbf{x}_{\text{lat}} = \begin{bmatrix} \omega_1 & \sigma_r & \theta & \vartheta & r & \omega_3 & \varepsilon \end{bmatrix}^\mathsf{T}, \quad u_{\text{lat}} = F, \\ \mathbf{x}_{\text{lon}} = \begin{bmatrix} \tilde{\omega}_2 & \tilde{\sigma}_{\gamma} & \gamma & \tilde{\varphi} & \tilde{s} \end{bmatrix}^\mathsf{T}, \quad u_{\text{lon}} = M, \end{cases}$$
(29)

where the tildes indicate perturbations for variables whose steady state values are not zero. Note that, this laterallongitudinal decomposition does not necessarily hold for turning-rolling type steady states.

The system and input matrices related to the lateral dynamics are

$$\mathbf{A}_{\text{lat}} = \begin{bmatrix} 0 & 0 & 0 & a_1 & a_2 & a_3 & 0 \\ 0 & 0 & 0 & -g & 0 & -R\dot{\varphi}_* & 0 \\ 0 & 0 & 0 & 0 & 0 & 1 & 0 \\ 1 & 0 & 0 & 0 & 0 & 0 & 0 \\ R & 1 & 0 & 0 & 0 & 0 & 0 \\ -2\dot{\varphi}_* & 0 & 0 & 0 & 0 & 0 & 0 \\ 0 & 0 & R\dot{\varphi}_* & 0 & 0 & 0 & 0 \end{bmatrix}, \quad \mathbf{B}_{\text{lat}} = \begin{bmatrix} b_1 \\ \frac{1}{m_1} \\ 0 \\ 0 \\ 0 \\ 0 \\ 0 \end{bmatrix}, (30)$$

where

$$a_{1} = 4g (mR + m_{2} (R + h))/c_{1}, a_{2} = -4m_{1}g/c_{1},$$

$$a_{3} = 2R\dot{\varphi}_{*} (3mR + m_{2} (2R + 2h))/c_{1}, b_{1} = 4R/c_{1},$$

$$c_{1} = 5mR^{2} + m_{2} \left(4R^{2} + 8Rh + 4h^{2}\right).$$
(31)

Similarly, the system and input matrices related to the longitudinal dynamics are

$$\mathbf{A}_{\text{lon}} = \begin{bmatrix} 0 & 0 & a_4 & 0 & 0 \\ 0 & 0 & g & 0 & 0 \\ -\frac{R}{h} & \frac{1}{h} & 0 & 0 & 0 \\ 1 & 0 & 0 & 0 & 0 \\ R & 0 & 0 & 0 & 0 \end{bmatrix}, \quad \mathbf{B}_{\text{lon}} = \begin{bmatrix} b_2 \\ \frac{1}{m_2 h} \\ 0 \\ 0 \\ 0 \end{bmatrix}, \tag{32}$$

where

$$a_4 = -2m_2g/(3mR + 2m_1R),$$

$$b_2 = -2(R+h)/(3mR^2h + 2m_1R^2h).$$
(33)

The structure of system matrix \mathbf{A}_{lat} shows that the lateral system states are not linearly independent. Similarly, the longitudinal system states are also not linearly independent. Let us choose the two sets of output states to be

$$\mathbf{y}_{\text{lat}} = \mathbf{C}_{\text{lat}} \mathbf{x}_{\text{lat}} := \begin{bmatrix} \omega_1 & \sigma_r & \theta & \vartheta & r & \varepsilon \end{bmatrix}^\mathsf{T}, \mathbf{y}_{\text{lon}} = \mathbf{C}_{\text{lon}} \mathbf{x}_{\text{lon}} := \begin{bmatrix} \tilde{\omega}_2 & \tilde{\sigma}_{\gamma} & \gamma & \tilde{s} \end{bmatrix}^\mathsf{T},$$
(34)

with appropriate output matrices C_{lat} and C_{lon} .

It can be shown that the lateral and longitudinal systems are output controllable with the control inputs F and M, respectively, as the output controllability matrices

$$\mathbf{M}_{\mathrm{oc},l} = \begin{bmatrix} \mathbf{C}_{l} \mathbf{B}_{l} & \mathbf{C}_{l} \mathbf{A}_{l} \mathbf{B}_{l} & \mathbf{C}_{l} \mathbf{A}_{l}^{2} \mathbf{B}_{l} & \dots \end{bmatrix}$$
(35)

have full ranks, i.e., rank $\mathbf{M}_{oc,lat} = 6$ and rank $\mathbf{M}_{oc,lon} = 4$.

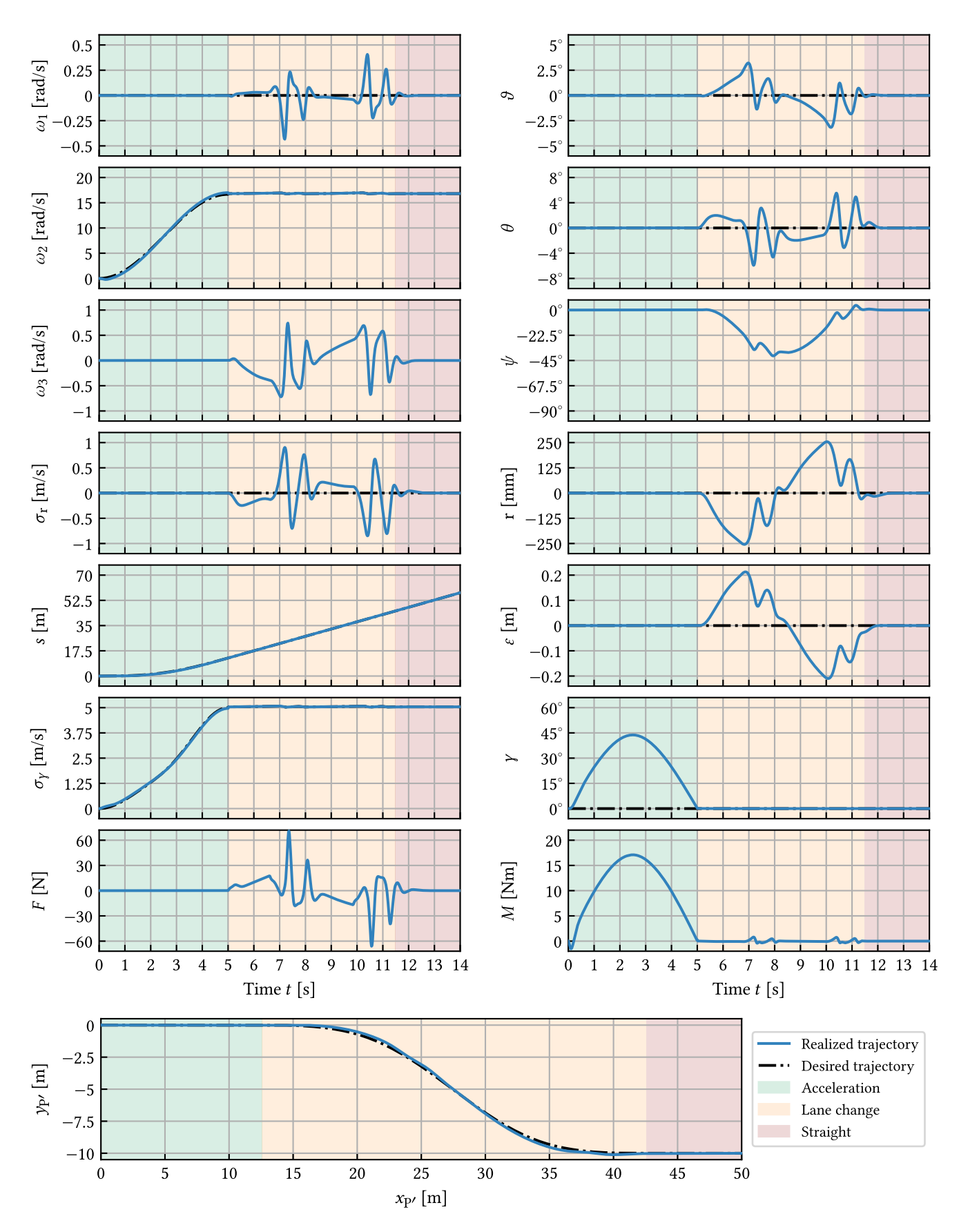


Fig. 3. Simulation results for a lane change maneuver

TABLE I PARAMETER VALUES

Quantity	Value	
Disc mass m	10	kg
Disc radius R	0.3	m
Fork length h	0.3	m
Gravitational acceleration g	9.81	m/s ²
Point mass m_1	10	kg
Point mass m_2	10	kg

In order to control the unicycle and to successfully track a predefined path with a prescribed velocity profile, we apply the linear feedback laws:

$$F := D_{\vartheta}\omega_{1} + D_{r}\sigma_{r} + P_{\theta}\theta + P_{\vartheta}\vartheta + P_{r}r + P_{\varepsilon}\varepsilon,$$

$$M := D_{\varphi}\hat{\omega}_{2} + D_{\gamma}\hat{\sigma}_{\gamma} + P_{\gamma}\gamma + P_{s}\hat{s}_{s},$$
(36)

where the errors are defined as

$$\hat{\omega}_2 = \omega_2 - \omega_{2,des}, \quad \hat{\sigma}_{\gamma} = \sigma_{\gamma} - \sigma_{\gamma,des}, \quad \hat{s} = s - s_{des}, \quad (37)$$

and $s_{des}(t)$ is the desired position along the trajectory, while

$$\omega_{2,\text{des}}(t) = R\dot{s}_{\text{des}}(t),$$

$$\sigma_{\gamma,\text{des}}(t) = \omega_{2,\text{des}}(t)R\cos\gamma(t) + \omega_3(t)h\tan\vartheta(t).$$
(38)

The control gains in (36) are chosen such that the resulting systems have all identical eigenvalues $\lambda_i = -12 \,\mathrm{s}^{-1}$.

V. SIMULATION RESULTS

The performance of the designed controller is tested via numerical simulation where the linear control laws (36) are applied to the nonlinear system (24). The simulation results are shown in Fig. 3, where the desired states and the desired path are shown by the dashed black curves, while the realized ones are depicted by the blue curves.

The desired trajectory is a lane change maneuver, which is divided into 3 sections. The first section is the acceleration phase: the unicycle starts at standstill, i.e., $v_{P'} = 0 \text{ m/s}$, and reaches $v_{P'} = 5 \text{ m/s}$ in 5 seconds, while running along the x_0 axis. The second section is the lane change, which consists of 3 clothoid segments to ensure continuous curvature $\kappa(s)$ along the trajectory. The third section is a straight line parallel to the x_0 axis. These sections are highlighted by different background colors in Fig. 3: acceleration with light green, lane change with light yellow, and the final straight section with light red.

The designed controller is capable to carry out the desired lane change maneuver with sufficiently small errors. The power requirements for this maneuver are below 30 W for the lateral actuator and below 200 W for the longitudinal actuator. These are in the realistic range for such a device, so input constraints do not need to be factored in. However, wheel slip and excessive tilt may occur, so state constraints will be important to consider in the future.

VI. CONCLUSION

The path-tracking control of an autonomous unicycle is considered in this work. A new mechanical model is introduced with two actuators for the lateral and longitudinal control. The governing equations are derived using the pseudovelocity based Appellian approach.

It is shown that the lateral and longitudinal dynamics can be decoupled. The three key factors to achieve this are: (a) utilizing 'smart' pseudo-velocity selections, (b) transforming the system to the trajectory reference frame, and (c) applying linearization around the straight line steady state motion.

Consequently, the lateral and longitudinal controls can be designed independently. Linear feedback laws were proposed for trajectory tracking. One limitation of the current work is that the desired states along the path were not planned. Generally, it is difficult to maneuver with the vertical wheel or accelerate with the vertical pendulum. Regardless, the proposed controller successfully performed the prescribed maneuver. The design of more feasible trajectories for the unicycle is the topic of future research.

REFERENCES

- [1] D. Zenkov, A. Bloch, and J. Marsden, "The Lyapunov-Malkin theorem and stabilization of the unicycle with rider," *Systems & Control Letters*, vol. 45, pp. 293–300, 2002. DOI: 10.1016/S0167-6911(01)00187-6.
- [2] D. W. Vos and A. H. von Flotow, "Dynamics and nonlinear adaptive control of an autonomous unicycle: Theory and experiment," in th IEEE Conference on Decision and Control, vol. 1, 1990, pp. 182–187. DOI: 10.2514/6.1990-1241.
- [3] A. R. Geist, J. Fiene, N. Tashiro, Z. Jia, and S. Trimpe, "The wheelbot: A jumping reaction wheel unicycle," *IEEE Robotics* and Automation Letters, vol. 7, no. 4, pp. 9683–9690, 2022. DOI: 10.1109/LRA.2022.3192654.
- [4] X. Cao, D. C. Bui, D. Takács, and G. Orosz, "Autonomous unicycle: Modeling, dynamics, and control," *Multibody System Dynamics*, vol. 61, no. 1, pp. 43–76, 2024. DOI: 10.1007/s11044-023-09923-7.
- [5] H. B. Brown and Y. Xu, "A single-wheel, gyroscopically stabilized robot," in *Proceedings of IEEE international conference on robotics and automation*, IEEE, vol. 4, 1996, pp. 3658–3663. DOI: 10.1109/100.618022.
- [6] A. Schoonwinkel, "Design and test of a computer stabilized unicycle," Ph.D. dissertation, Stanford University, 1987.
- [7] K. G. Gim and J. Kim, "Ringbot: Monocycle robot with legs," IEEE Transactions on Robotics, vol. 40, pp. 1890–1905, 2024. DOI: 10.1109/TRO.2024.3362326.
- [8] H. Suzuki, S. Moromugi, and T. Okura, "Development of robotic unicycles," *Journal of Robotics and Mechatronics*, vol. 26, no. 5, pp. 540–549, 2014. DOI: 10.20965/jrm.2014.p0540.
- [9] M. B. Vizi, G. Orosz, D. Takács, and G. Stépán, "Steering control of an autonomous unicycle," *IEEE Transactions on Control Systems Technology*, 2023, (under review). [Online]. Available: arxiv.org/abs/2307.08387.
- [10] M. B. Vizi, G. Orosz, D. Takács, and G. Stépán, "Maneuvering an autonomous spatial unicycle," *IFAC-PapersOnLine*, vol. 58, no. 28, pp. 438–443, 2024. DOI: 10.1016/j.ifacol.2025.01.085.
- [11] P. Appell, "Sur une forme générale des équations de la dynamique (On a general form of the equations of dynamics)," *Journal für die reine und angewandte Mathematik (Journal for Pure and Applied Mathematics)*, vol. 121, pp. 310–319, 1900. DOI: 10.1515/crll.1900.121.310.
- [12] E. Desloge, "The Gibbs-Appell equations of motion," *American Journal of Physics*, vol. 56, pp. 841–846, 1988. DOI: 10.1119/1.15463.
- [13] W. B. Qin, Y. Zhang, D. Takács, G. Stépán, and G. Orosz, "Non-holonomic dynamics and control of road vehicles: Moving toward automation," *Nonlinear Dynamics*, vol. 110, no. 3, pp. 1959–2004, 2022. DOI: 10.1007/s11071-022-07761-4.
- [14] G. Csernák, "Analysis of pole acceleration in spatial motions by the generalization of pole changing velocity," *Acta Mechanica*, vol. 230, no. 7, pp. 2607–2624, 2019. DOI: 10.1007/s00707-019-02408-9.